Available online at www.sciencedirect.com
SCIENCE DIRECT®
Journal of Solid State Chemistry 178 (2005) 1988–1995
JOURNAL OF SOLID STATE CHEMISTRY
www.elsevier.com/locate/jssc

Controlled assembly of two new bicapped bisupporting Keggin-polyoxometalate derivatives: $[M(2,2'\text{-bpy})_2(H_2O)]_2[SiMo^{VI}{}_8Mo^{V}{}_4V^{IV}{}_2O_{42}]$ (M = Co, Zn)

Zhenyu Shi, Xiaojun Gu, Jun Peng*, Yanhui Chen

[a]*Institute of Polyoxometalate Chemistry, Department of Chemistry, Northeast Normal University, Changchun, 130024, PR China*

Received 9 March 2005; received in revised form 2 April 2005; accepted 6 April 2005

Abstract

Two new neutral bicapped bisupporting Keggin-polyoxometalate derivatives: $[M(2,2'\text{-bpy})_2(H_2O)]_2[SiMo^{VI}{}_8Mo^{V}{}_4V^{IV}{}_2O_{42}]$ (M = Co **1**, Zn **2**; 2,2′-bpy = 2,2′-bipyridine), have been synthesized under hydrothermal conditions by directly using $H_4SiMo_{12}O_{40}$ as starting materials. Crystal data for compound **1**: $C_{40}H_{36}Co_2Mo_{12}N_8O_{44}SiV_2$, triclinic, space group $P\bar{1}$, $a = 11.884(2)$ Å, $b = 12.459(3)$ Å, $c = 12.652(3)$ Å, $\alpha = 71.02(3)^\circ$, $\beta = 74.51(3)^\circ$, $\gamma = 86.74(3)^\circ$, $V = 1706.3(6)$ Å^3, $Z = 1$; for compound **2**, $C_{40}H_{36}Mo_{12}N_8O_{44}SiV_2Zn_2$, triclinic, space group $P\bar{1}$, $a = 11.879(2)$ Å, $b = 12.469(3)$ Å, $c = 12.635(3)$ Å, $\alpha = 71.28(3)^\circ$, $\beta = 74.78(3)^\circ$, $\gamma = 86.60(3)^\circ$, $V = 1709.6(6)$ Å^3, $Z = 1$. The studies of the electrochemical property of compounds **1** and **2** exhibit similar redox behavior to the parent $[(C_4H_9)_4N]_4SiMo_{12}O_{40}$, undergoing three two-electron reversible reductions. Variable-temperature magnetic susceptibility measurement of compound **1** demonstrates the presence of antiferromagnetic interactions.

Keywords: Bicapped Keggin; Polyoxometalate; Hydrothermal synthesis; Electrochemical property; Magnetic property

1. Introduction

Inorganic–organic hybrid materials have recently attracted great interest because of their diverse structural flexibility and potential applications in molecular absorption, biology, photochemistry and electromagnetism [1–8]. An attractive challenge in this field is the design and synthesis of novel solid materials based on polyoxometalates (POMs). To date, a number of transition metal coordination complex-linking POMs with zero-, one-, two- and three-dimensional frameworks have been synthesized [9–15]. Among these compounds, capped Keggin POMs are especially arrestive owing to their particular properties and applications in medicine and electrocatalysis. However, discrete capped Keggin POMs decorated by transition metal complexes are still much less exploited. Up to now, only several examples have been reported, such as tetracapped tetrasupporting $[PMo^{VI}{}_6Mo^{V}{}_2V^{IV}{}_8O_{44}\ \{Co(2,2'\text{-bpy})_2(H_2O)\}_4]^{3+}$ [9] and $[Mo^{VI}{}_7Mo^{V}V^{IV}{}_8O_{40}(PO_4)][Co(phen)_2(OH)_2][Co(phen)_2(OEt)]_2$ (phen = 1,10′-phenanthroline, OEt = ethanol) [16], the sole bicapped bisupporting anion $[PMo^{VI}{}_8V^{IV}{}_6O_{42}\{Cu(phen)\}_2]^{5-}$ [9], and bicapped monosupporting $[PMo^{VI}{}_8V^{IV}{}_6O_{42}Cu(en)(phen)]^{5-}$ (en = ethylenediamine) [17]. Furthermore, all these compounds were obtained from simple inorganic oxides or salts. To our knowledge, discrete capped Keggin-POMs decorated by transition metal complexes, which are constructed directly from pre-synthesized Keggin POM building blocks under hydrothermal conditions, have never been reported.

Recently, POMs are very attractive in electrode modification and electrocatalytic research because of

*Corresponding author. Fax: +86 431 568 4009.
E-mail addresses: jpeng@nenu.edu.cn, pjun56@yahoo.com (J. Peng).

0022-4596/$ - see front matter © 2005 Elsevier Inc. All rights reserved.
doi:10.1016/j.jssc.2005.04.005

their ability to undergo reversible multi-electron redox process [18]. Some strategies, such as absorption and electrodeposition, have been explored to fabricate chemically modified electrodes with POMs (CMEP) [19,20]. These traditional CMEP take advantage of the good solubility of POMs in solutions. However, POM-based organic–inorganic hybrids synthesized by hydrothermal technique are usually insoluble in water or common organic solvents. So their electrochemical properties cannot be measured by the methods mentioned above. For both a better understanding of the electrochemical property and expanding of POM-based materials' application, a chemically modified carbon paste electrode (CPE) opens up a good way to study the electrochemical behavior of POM-based compounds with poor solubility in water and most solvents [21]. Chemically modified CPE is a mixture of a modifier, graphite power and pasting liquid. And the modifiers used to direct mixing should be insoluble in the analytic solution in order to avoid dissolution of the molecules from the electrode surface during the measurement.

Our interest is the target synthesis of Keggin POM-based solids by hydrothermal technique. In previous work, we have synthesized two two-dimensional layered POM-based compounds by directly using pre-synthesized Keggin POM building blocks and 1,10′-phenanthroline as ligand [22]. In order to further understand the ligand influences on the structures of such compounds, we substituted 2,2′-bpy for 1,10′-phenanthroline. Herein, we report the hydrothermal syntheses, characterization, electrochemical properties and magnetic property of another such synthesized example, two neutral bicapped bisupporting Keggin-POM derivatives: $[M(2,2'\text{-bpy})_2(H_2O)]_2[SiMo^{VI}{}_8Mo^{V}{}_4V^{IV}{}_2O_{42}]$ (M = Co **1**, Zn **2**). Interestingly, unlike those previous reported capped supporting POMs, the intact skeletons of Keggin POM in compounds **1** and **2** are still maintained in the final products. To our knowledge, they represent the first example of neutral bicapped bisupporting Keggin POMs.

2. Experimental section

2.1. General procedures

All reagents were purchased commercially and used without further purification. Elemental analyses (C, H and N) were performed on a Perkin-Elmer 2400 CHN Elemental Analyzer. Co, Zn, Mo and V were determined by a Leaman inductively coupled plasma (ICP) spectrometer. IR spectra were obtained on Alpha Centaurt FT/IR spectrometer with KBr pellet in the 400–4000 cm^{-1} region. XPS analyses were performed on a VG ESCALAB MK II spectrometer with a Mg-$K\alpha$ (1253.6 eV) achromatic X-ray source. The vacuum inside the analysis chamber was maintained at 6.2×10^{-6} Pa during analysis. The ESR spectrum was recorded on a Japanese JES-FE3AX spectrometer at room temperature. The TG analyses were performed on a Perkin-Elmer TGA7 instrument in flowing N_2 with a heating rate of 10 °C min^{-1}. Cyclic voltammograms were obtained with a CHI 660 electrochemical workstation at room temperature. A platinum gauze was used as counter electrode and an Ag/AgCl was used as reference electrode. A chemically bulk-modified CPE was used as working electrode. The magnetic susceptibility measurement for compound **1** was carried out using a Quantum Design MPMS-XL SQUID magnetometer at 1000 G. Diamagnetic correction was estimated from Pascal's constants [23].

2.2. Syntheses of compounds $[Co(2,2'\text{-bpy})_2(H_2O)]_2[SiMo^{VI}{}_8Mo^{V}{}_4V^{IV}{}_2O_{42}]$ (**1**) and $[Zn(2,2'\text{-bpy})_2(H_2O)]_2[SiMo^{VI}{}_8Mo^{V}{}_4V^{IV}{}_2O_{42}]$ (**2**)

Compounds **1** and **2** were synthesized hydrothermally from a mixture of $H_4[SiMo_{12}O_{40}]\cdot xH_2O$ [24] (0.25 mmol), $M(NO_3)_2\cdot 6H_2O$ (M = Co, Zn) (0.25 mmol), NH_4VO_3 (0.5 mmol), 2,2′-bpy (0.25 mmol), triethylamine (1.0 mmol) and H_2O (9.0 ml) in a molar ratio 1:1:2:1:4:2000. The resulting suspension was stirred for 1 h, sealed in an 18 ml Teflon-lined reactor and heated at 160 °C for 6 days. Black block crystals were filtered, washed with water, and dried at room temperature (yield 56%, **1**; 47%, **2** based on molybdenum). $C_{40}H_{36}Co_2Mo_{12}N_8O_{44}SiV_2$ (2731.8) **1**: Elemental analyses: found: C, 17.31%; H, 1.39%; N, 4.07%; Co, 4.38%; Mo, 42.31%; V, 3.62%. Calc.: C, 17.59%; H, 1.32%; N, 4.10%; Co, 4.31%; Mo, 42.14%; V, 3.73%. $C_{40}H_{36}Mo_{12}N_8O_{44}SiV_2Zn_2$ (2744.7) **2**, Found: C, 17.28%, H, 1.37%, N, 4.11%, Zn, 4.64%, Mo, 42.02%, V, 3.66%. Calc.: C, 17.50%; H, 1.31%, N, 4.08%; Zn, 4.76%; Mo, 41.95%, V, 3.71%. Selected FTIR data (cm^{-1}): For **1**, 1622 (m), 1569 (m), 1470 (m), 1440 (s), 1175 (m), 949 (s), 880 (s), 790 (s), 760 (s), 734 (s); for **2**, 1602 (m), 1560 (m), 1473 (m), 1443 (s), 1152 (m), 952 (s), 880 (s), 762 (s).

2.3. X-ray crystallography

Crystal data for compounds **1** and **2** were collected on Rigaku R-AXIS RAPID IP and Bruker SMART-CCD diffractometer with Mo-$K\alpha$ monochromated radiation (λ = 0.71073 Å) at 293 K, respectively. The structure was solved by the directed methods and refined by full-matrix least-squares on F^2 using the SHELXTL crystallographic software package [25]. All the non-hydrogen atoms were refined anisotropically. The hydrogen atoms were located from difference Fourier maps and were refined isotropically. The crystal data and structure refinement of compounds **1** and **2** were summarized in

Table 1
Crystal data and structure refinement of compounds **1** and **2**

Compounds	**1**	**2**
Empirical formula	$C_{40}H_{36}Co_2Mo_{12}N_8O_{44}SiV_2$	$C_{40}H_{36}Mo_{12}N_8O_{44}SiV_2Zn_2$
Formula weight	2731.8	2744.7
Temperature (K)	293	293
Crystal system	Triclinic	Triclinic
Space group	$P\bar{1}$	$P\bar{1}$
a (Å)	11.884(2)	11.879(2)
b (Å)	12.459(3)	12.469(3)
c (Å)	12.652(3)	12.635(3)
α (deg)	71.02(3)	71.28(3)
β (deg)	74.51(3)	74.78(3)
γ (deg)	86.74(3)	86.60(3)
V (Å^3)	1706.3(6)	1709.6(6)
Z	1	1
λ (Å)	0.71073	0.71073
D_c/Mg (m^{-3})	2.655	2.662
μ (mm)$^{-1}$	2.977	3.188
F(000)	1298	1304
Reflection collected	15417	13623
Independent reflections	7334	6101
Absorption correction	Empirical	Empirical
Refinement method	Full-matrix least-squares on F^2	Full-matrix least-squares on F^2
$R1$, wR_2 [$I>2\sigma(I)$]	0.0599, 0.1382	0.0479, 0.1146
$R1$, wR_2 (all data)	0.0760, 0.1448	0.0526, 0.1165

Table 1. Selected bond lengths and angles were listed in Tables 2 and 3.

2.4. Preparation of *1*-, *2*-CPE and *{[(C4H9)4N]4SiMo12O40}*-CPE

Two hundred milligrams of graphite powder and ca. 40 mg **1** (**2** or $\{[(C_4H_9)_4N]_4SiMo_{12}O_{40}\}$) were mixed and ground together by agate mortar and pestle to achieve an even, dry mixture. To the mixture, 0.26 ml nujol was added and stirred with a glass rod. Then the homogenized mixture was used to pack 3 mm inner diameter glass tubes, and the surface was wiped with weighing paper. Electrical contact was established with copper rod through the back of the electrode.

3. Results and discussion

3.1. Crystal structures

Compounds **1** and **2** were prepared by hydrothermal reactions. Single crystal X-ray diffraction study reveals that **1** is a neutral bicapped bisupporting POM: $[Co(2,2'\text{-bpy})_2(H_2O)]_2[SiMo^{VI}{}_8Mo^{V}{}_4V^{IV}{}_2O_{42}]$. As shown in Fig. 1, Compound **1** is composed of a bicapped Keggin $[SiMo^{VI}{}_8Mo^{V}{}_4V^{IV}{}_2O_{42}]^{4-}$ unit and two $\{Co(2,2'\text{-bpy})_2(H_2O)\}$ fragments. The $[SiMo^{VI}{}_8Mo^{V}{}_4V^{IV}{}_2O_{42}]^{4-}$ cluster

Table 2
Selected bond lengths (Å) and angles (deg) for compound **1**

Mo(1)–O(13)	1.637(6)	Co(1)–O(12)	2.049(6)
Mo(1)–O(18)	1.913(7)	Co(1)–Ow1	2.243(6)
Mo(1)–O(21)	1.926(7)	Co(1)–N(1)	2.124(7)
Mo(1)–O(1)	2.406(9)	Co(1)–N(2)	2.101(6)
Mo(1)–O(3)#	2.470(9)	Co(1)–N(3)	2.105(7)
Mo(1)–O(5)#	1.920(8)	Co(1)–N(4)	2.099(7)
Mo(1)–O(6)#	1.927(8)	V(1)–O(12)	1.620(5)
Mo(2)–O(17)	1.656(6)	V(1)–O(11)	1.920(6)
Mo(2)–O(18)	1.811(6)	V(1)–O(19)	1.919(6)
Mo(2)–O(11)	2.027(6)	V(1)–O(15)	1.930(6)
Mo(2)–O(22)	1.815(7)	V(1)–O(14)	1.922(6)
Mo(2)–O(2)#	2.426(1)	Si(1)–O(3)	1.607(9)
Mo(2)–O(3)#	2.429(1)	Si(1)–O(4)	1.646(9)
Mo(2)–O(14)	2.038(6)	Si(1)–O(1)	1.654(9)
Si(1)–O(2)	1.602(1)		
O(18)–Mo(1)–O(13)	100.7(4)	O(17)–Mo(2)–O(2)#	158.2(4)
O(13)–Mo(1)–O(21)	101.2(4)	O(11)–Mo(2)–O(14)	75.0(2)
O(18)–Mo(1)–O(5)#	157.7(5)	O(17)–Mo(2)–O(22)	103.4(4)
O(18)–Mo(1)–O(21)	87.2(3)	O(11)–Mo(2)–O(22)	90.6(3)
O(1)–Mo(1)–O(13)	157.8(3)	O(12)–V(1)–O(19)	114.4(4)
O(1)–Mo(1)–O(18)	96.1(4)	O(19)–V(1)–O(11)	80.5(3)
O(13)–Mo(1)–O(3)#	157.4(3)	O(19)–V(1)–O(14)	130.3(4)
O(18)–Mo(1)–O(3)#	63.5(3)	O(12)–V(1)–O(15)	113.4(3)
O(1)–Mo(1)–O(6)#	64.5(4)	O(15)–V(1)–O(19)	79.9(3)
O(21)–Mo(1)–O(3)#	63.8(3)	O(12)–Co(1)–N(4)	96.0(3)
O(13)–Mo(1)–O(6)#	101.1(4)	O(12)–Co(1)–N(2)	91.0(2)
N(2)–Co(1)–N(1)	76.3(3)	N(4)–Co(1)–N(3)	78.0(3)
N(2)–Co(1)–OW	97.0(3)	N(4)–Co(1)–OW	90.1(3)
O(3)–Si(1)–O(4)#	109.1(5)	O(1)–Si(1)–O(3)	110.5(5)
O(2)–Si(1)–O(3)#	110.7(5)	O(4)–Si(1)–O(2)	112.2(5)

Table 3
Selected bond lengths (Å) and angles (deg) for compound **2**

Mo(1)–O(9)	1.657(5)	Zn(1)–O(21)	2.056(5)
Mo(1)–O(8)	1.815(7)	Zn(1)–Ow1	2.305(6)
Mo(1)–O(6)	1.816(8)	Zn(1)–N(1)	2.103(7)
Mo(1)–O(15)	2.033(6)	Zn(1)–N(2)	2.129(7)
Mo(1)–O(23)	2.057(6)	Zn(1)–N(3)	2.162(7)
Mo(1)–O(2)	2.378(9)	Zn(1)–N(4)	2.109(6)
Mo(1)–O(3)	2.449(9)	V(1)–O(21)	1.619(5)
Mo(2)–O(14)	1.647(6)	V(1)–O(23)	1.918(6)
Mo(2)–O(7)#	1.908(7)	V(1)–O(17)	1.920(6)
Mo(2)–O(11)	1.909(7)	V(1)–O(15)	1.921(6)
Mo(2)–O(8)	1.935(7)	V(1)–O(22)	1.927(6)
Mo(2)–O(5)#	1.953(7)	Si(1)–O(3)	1.609(9)
Mo(2)–O(1)#	2.407(1)	Si(1)–O(4)	1.614(1)
Mo(2)–O(3)	2.468(1)	Si(1)–O(1)	1.641(1)
Si(1)–O(2)	1.655(1)		
O(8)–Mo(1)–O(9)	102.8(4)	O(14)–Mo(2)–O(1)#	156.9(4)
O(6)–Mo(1)–O(9)	101.9(4)	O(11)–Mo(2)–O(8)	86.4(3)
O(6)–Mo(1)–O(8)	96.4(4)	O(14)–Mo(2)–O(11)	103.8(4)
O(9)–Mo(1)–O(15)	97.6(3)	O(11)–Mo(2)–O(7)#	90.1(4)
O(8)–Mo(1)–O(15)	156.4(3)	O(21)–V(1)–O(23)	115.3(3)
O(9)–Mo(1)–O(23)	97.3(3)	O(17)–V(1)–O(15)	130.5(4)
O(15)–Mo(1)–O(23)	74.8(2)	O(23)–V(1)–O(17)	80.2(3)
O(9)–Mo(1)–O(2)	155.0(3)	O(21)–V(1)–O(15)	114.0(3)
O(3)–Mo(1)–O(9)	156.0(3)	O(21)–V(1)–O(22)	113.3(3)
O(6)–Mo(1)–O(3)	100.4(5)	O(21)–Zn(1)–N(1)	94.8(3)
O(2)–Mo(1)–O(3)	46.8(3)	N(1)–Zn(1)–N(4)	169.7(3)
N(1)–Zn(1)–N(2)	78.3(3)	O(21)–Zn(1)–N(4)	92.5(2)
N(1)–Zn(1)–N(3)	95.8(3)	O(21)–Zn(1)–Ow1	87.0(2)
O(3)–Si(1)–O(4)#	111.3(5)	O(1)–Si(1)–O(3)	112.6(5)
O(4)–Si(1)–O(1)#	108.5(5)	O(4)–Si(1)–O(2)	110.2(5)

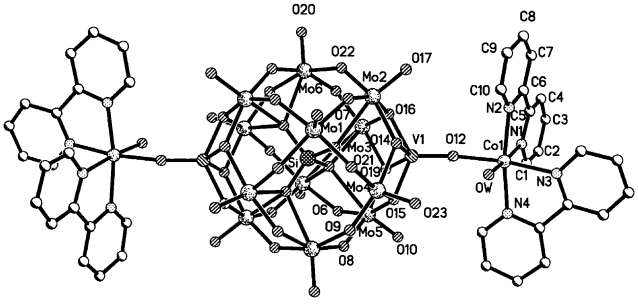

Fig. 1. View of the structure of the POM $[Co(2,2'\text{-bpy})_2(H_2O)]_2[SiMo^{VI}{}_8Mo^{V}{}_4V^{IV}{}_2O_{42}]$ in compound **1**. Only parts of atoms are labeled and all H atoms are omitted for clarity.

is similar to that in $(Et_3NH)_5[PMo^{V}{}_6Mo^{VI}{}_6O_{40}(V^{IV}O)_2]$ (Et_3N = triethylamine) [26], and identical with that in $\{[Co(phen)_2]_2[SiMo^{VI}{}_8Mo^{V}{}_4O_{40}(V^{IV}O)_2]\}\{[Co(phen)_2(H_2O)]_2[SiMo^{VI}{}_8Mo^{V}{}_4O_{40}(V^{IV}O)_2]\}\cdot 3H_2O$ [22] recently reported by us. It can be described as bicapped Keggin structure, namely, one α-Keggin core $\{SiMo_{12}O_{40}\}$ with $\{VO\}$ units capping two opposite pits. The central atom Si is located at the inversion center, which results in a disordered SiO_4 tetrahedron, namely, the central atom Si is surrounded by a cube of eight oxygen atoms, with each oxygen site half-occupied. The Si–O average distance is 1.628(0) Å and O–Si–O bond angles are in the range 105.3(5)–112.2(5)°. There is only one crystallographically unique vanadium center. The vanadium atom exhibits a distorted $\{VO_5\}$ square pyramidal environment with V–O distances in the range 1.620(5)–1.930(6) Å and bond angles 79.8(3)–131.7(4)°. All molybdenum atoms have a distorted $\{MoO_6\}$ octahedral environment. The distances of Mo–O bonds are divided in three groups: Mo–O_a, 2.363(9)–2.471(1) Å, Mo–O_b, 1.805(7)–2.052(6) Å, Mo–O_t, 1.637(6)–1.665(6) Å, which are comparable with those in $[PMo^{VI}{}_8V^{IV}{}_6O_{42}\{Cu(phen)\}_2]^{5-}$ [Mo–O_a, 2.385(9)–2.486(1) Å, Mo–O_b, 1.787(5)–2.062(5) Å, Mo–O_t, 1.668(5)–1.679(6) Å] [9]. The assignments of oxidation state for the molybdenum and vanadium are consistent with their coordination geometries and confirmed by valence sum calculations [27]. The valence sum calculations show that all vanadium atoms are in the 4+ oxidation state, while four molybdenum atoms are in the 5+ oxidation state. In comparison with other bicapped Keggin polyoxoanions, the unusual feature of compound **1** is that the skeleton of classical Keggin POM is fully maintained. It should be noted that the maintenance of skeletons of Keggin POMs seemed to be simple, but it turned out to be a challenging goal under hydrothermal conditions. The successful syntheses of such compounds show that controlled assembly of Keggin POM-based compounds can be realized under hydrothermal conditions by rationally tuning reaction conditions.

A μ_2-oxygen O(12) joins the bicapped Keggin unit to $\{Co(2,2'\text{-bpy})_2(H_2O)\}$ fragment with Co(1)–O(12) distance of 2.049(6) Å. The Co(1) atom is coordinated by one oxygen atom O(12), one water molecule with Co–Ow distance of 2.243(6), and four nitrogen atoms from two 2,2′-bpy ligands with Co–N distances of 2.099(7)–2.124(7) Å.

In compound **1**, each bicapped bisupporting POM cluster joins other neighboring clusters through hydrogen

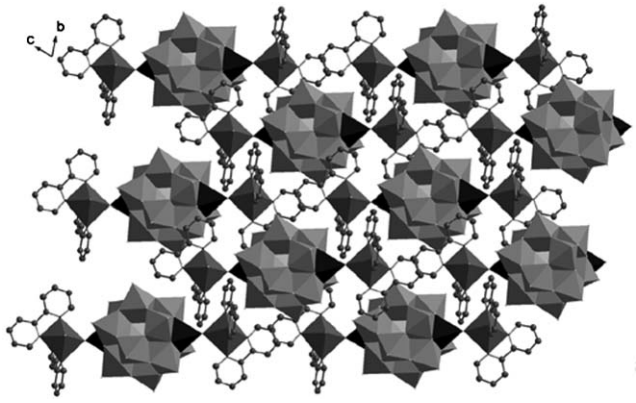

Fig. 2. Polyhedral representation of the three-dimensional structure in compounds **1** and **2**. All C, H atoms are omitted for clarity.

bonding interactions with the shortest O···O distance of 3.000 Å, thus resulting in an interesting three-dimensional supramolecular array (Fig. 2).

Compound **2** is isostructural with compound **1**. The Mo–O and V–O bond lengths [Mo–O_t 1.632(2)–1.669(2) Å, Mo–O_b 1.791(6)–2.083(9) Å, Mo–O_c 2.327(9)–2.498(8) Å, V–O_t 1.633(3)–1.637(4) Å, V–O_b 1.905(5)–1.940(6) Å] are comparable with those in **1**. The coordination mode of Zn atom is identical with Co(1) atom in compound **1**, exhibiting a distorted octahedral geometry in the form of $\{ZnN_4O_2\}$. The Zn–N distances are in the range of 2.103(7)–2.162(7) Å. Zn–O and Zn–Ow distances are 2.056(5) and 2.305(6) Å, respectively. All these bond distances and bond angles are within the normal ranges and in close agreement with those described in the literatures [9,16].

3.2. IR spectra, XPS spectra, TG analysis

In the IR spectra, the vibration modes for $\nu(Mo=O_t)$, $\nu(M–O_b–M)$, and $\nu(M–O_c–M)$ (M = V or Mo) occur at 949, 880, 760 cm^{-1} for **1**; 952, 880, 762 cm^{-1} for **2**, while bands at 1622, 1569, 1470, 1440 cm^{-1} in the IR spectrum of **1** and 1602, 1560, 1473, 1443 cm^{-1} in the IR spectrum of **2** are characteristic absorption of 2,2′-bpy ligands. The strong broad band around 3439 cm^{-1} in both IR spectra could be ascribed to absorption of coordinated water molecules. The EPR spectrum of compounds **1** and **2** exhibit the V^{4+} signal at 293 K with $g = 1.9976$ and 1.9944, respectively. No Mo^{5+} signal is found owing to electron delocalization. The XPS spectrum gives a peak at 516.2 eV attributed to V^{4+} and two overlapped peaks at 232.1 and 231.4 eV attributed to Mo^{6+} and Mo^{5+}. All these results further confirm the structure analysis.

Thermogravimetric (TG) curves of compounds **1** and **2** support their chemical compositions. Both indicate two steps of weight loss. The first weight loss in the temperature range 110–280 °C is corresponding to the release of the ligand water molecules, 1.24% (calc. 1.32%), **1**; 1.38 (calc. 1.31), **2**. The second weight loss at 280–500 °C is ascribed to decomposition of 2,2′-bpy ligands, 22.68% (calc. 22.84%), **1**; 22.79 (calc. 22.73), **2**.

3.3. Cyclic voltammetry

Compounds **1** and **2** are insoluble in water and most organic solvents, so we used them as modifiers to fabricate chemically modified CPE. Intact Keggin skeletons in compounds **1** and **2** are still maintained, therefore their electrochemical properties are expected to behave like their parent $H_4SiMo_{12}O_{40}$. Since $H_4SiMo_{12}O_{40}$ is soluble in water, insoluble salt of $[(C_4H_9)_4N]_4SiMo_{12}O_{40}$ **3** was prepared so that the comparison of electrochemical behavior between **3** and **1** (or **2**) could be done under identical conditions. In addition, the differences of electrochemical property brought about by the presence of $[Co(2,2'\text{-bpy})_2]^{2+}$ complex fragment instead of $[Zn(2,2'\text{-bpy})_2]^{2+}$ were selected as a basis for further comparisons. In short, three issues were found pertinent for this electrochemical study: (1) the redox behavior of parent **3**, (2) the redox behavior of compound **1** and the comparative cyclic voltammograms of compounds **1** and **3**, (3) the influence of complex fragments.

3.3.1. Voltammetric behavior of the parent 3-CPE

Fig. 3 shows the typical cyclic voltammetric behavior of **3**-CPE in 0.2 M $Na_2SO_4 + H_2SO_4$ (pH = 2.9) solution at different scan rates. In the potential range from 600 to −460 mV, three reversible redox peaks appear and the mean peak potentials $E_{1/2} = (E_{cp} + E_{ap})/2$ are +112, −44 and −214 mV, respectively. Each pair of redox peaks can be ascribed to two-electron process of molybdenum. With the scan rate varying from 20 to 200 mV s^{-1}, the peak potentials change gradually: the cathodic peak potentials shift toward the negative direction and the corresponding anodic peak potentials to the positive direction. It should be pointed out the peak-to-peak separation between the corresponding cathodic and anodic peaks increases with the scan rate increasing. This is common phenomenon for CPE [28]. Compared with the traditional CMEP, it can be concluded that for CPE with POM, the electron exchange rate between the insoluble solid **3** and electrode decreases owing to a slowdown of the penetration rate of protons from solution into particles.

3.3.2. Voltammetric behavior of 1-CPE

Fig. 4 illustrates the cyclic voltammetric behavior of **1**-CPE under identical conditions with **3**-CPE. Similarly

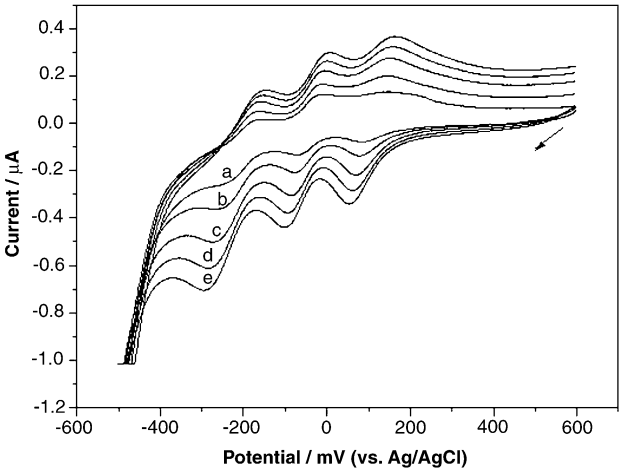

Fig. 3. Cyclic voltammograms of the **3**-CPE in the 0.2 M $Na_2SO_4 + H_2SO_4$ (pH = 2.9) solution at different scan rates: (a) 20, (b) 50, (c) 100, (d) 150 and (e) 200 mV s^{-1}. Potentials measured vs. Ag/AgCl.

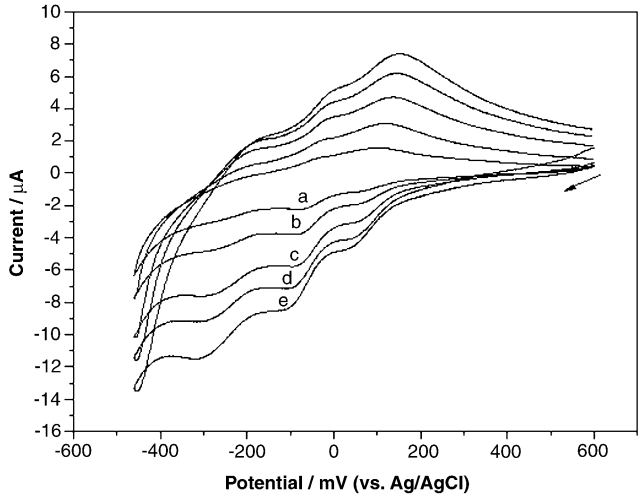

Fig. 4. Cyclic voltammograms of the **1**-CPE in the 0.2 M $Na_2SO_4+H_2SO_4$ (pH = 2.9) solution at different scan rates: (a) 20, (b) 50, (c) 100, (d) 150 and (e) 200 mV s^{-1}.

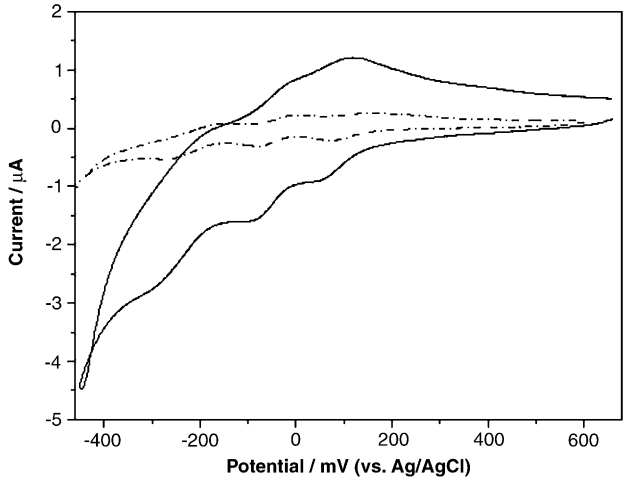

Fig. 5. Comparative cyclic voltammograms of (a) **3**-CPE (dotted line) and (b) **1**-CPE (solid line) in the 0.2 M $Na_2SO_4+H_2SO_4$ (pH = 2.9) solution. Scan rate: 100 mV s^{-1}.

to the **3**-CPE, there exist three pairs of reversible redox peaks. Furthermore, with the scan rates increasing, the cathodic peak potentials also shift toward the negative direction and the corresponding anodic peak potentials to the positive direction. The mean peak potentials $E_{1/2}$ are +96, −49 and −231 mV, respectively. The values of $E_{1/2}$ in **1**-CPE shift to the negative direction as compared with its parent **3**-CPE. No reduction of the "grafting" metallic cations (Co and V) have been detected in the potential domain studied.

For better understanding the difference and similarity of electrochemical properties between compounds **1** and **3**, Fig. 5 shows comparative cyclic voltammograms of **3**-CPE and **1**-CPE in 0.2 M $Na_2SO_4+H_2SO_4$ (pH = 2.9) solution at scan rate of 100 mV s^{-1}. It shows a ~15 mV negative shift for the first Mo^{VI} reduction peak potential in **1**-CPE compared with its parent **3**-CPE. But in general, the electrochemical behavior of **3**-CPE and **1**-CPE is very similar. This similarity can be explained as follows: (1) In compound **1**, the intact skeleton of Keggin POM is still maintained. So the influence of the structural difference between compounds **1** and **3** on electrochemical behavior is very little. (2) Generally, in a mixed Mo^{VI}/V^{V} polyoxoanion, the V^{V} centers are commonly reduced in the first place and then Mo centers are reduced [29]. However, the capped V centers in compound **1** are already in the +4 oxidation state. In view of these facts, the three reduction processes were assigned to $Mo^{VI}\rightarrow Mo^{V}$, similar to **3**. In a word, the VO^{2+} cap has a slight effect on the electrochemical property of **1**-CPE.

3.3.3. *Influence of the complex fragments on the electrochemical properties of **1**-CPE and **2**-CPE*

As shown in Fig. 6, the peak potentials for the three pairs of molybdenum redox peaks are hardly displaced, irrespective of whether the complex fragment is $[Co(2,2'\text{-bpy})_2]^{2+}$ or $[Zn(2,2'\text{-bpy})_2]^{2+}$. The values of $E_{1/2}$ in **2**-CPE are +103, −46 and −223 mV, respectively, close to those of **1**-CPE (+96, −49 and −231 mV). The small difference in $E_{1/2}$ of compounds **1** and **2** suggests Keggin core $\{SiMo_{12}O_{40}\}$ is the active center for electrochemical redox activity in CPE, while the corresponding complex fragments have only a slight influence on electrochemical behavior of **1**- or **2**-CPE.

3.4. *Magnetic property*

The thermal variation of the product of the molar magnetic susceptibility times the temperature, $\chi_m T$ for

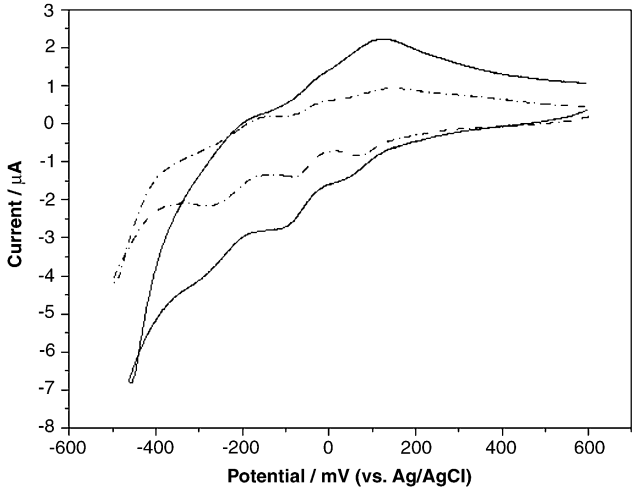

Fig. 6. Comparative cyclic voltammograms of (a) **1**-CPE (solid line) and (b) **2**-CPE (dotted line) in the 0.2 M $Na_2SO_4+H_2SO_4$ (pH = 2.9) solution. Scan rate: 100 mV s^{-1}.

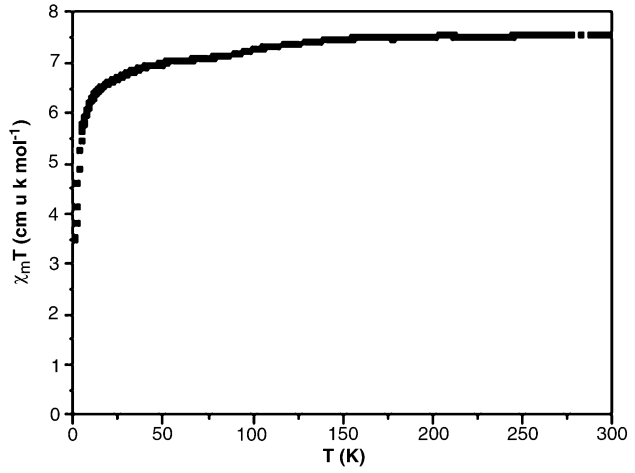

Fig. 7. Plots of the temperature dependence of $\chi_m T$ for compound **1**.

compound **1** shows a value 7.5 emu K mol^{-1} at 300 K and a continuous and smooth decrease when the temperature is lowered to reach a value of 6.9 emu K mol^{-1} at ca. 40 K. (Fig. 7). Below this temperature, $\chi_m T$ shows an abrupt decrease and reaches to a value of ca. 3.4 emu K mol^{-1} at 2 K. Assuming that the reduced molybdenum atoms do not contribute to the magnetic moment at room temperature, since the electrons are delocalized over all the POM (see ESR results) and assuming a contribution of ca. 0.75 emu K mol^{-1} for the two V(IV) ions (2×0.375 emu K mol^{-1} for $g = 2$), we can estimate a contribution of ca. 3.37 emu K mol^{-1} (5.19 B.M.) for each Co(II) complex. This value is very similar to those obtained for other octahedral Co(II) complexes and is within the expected range of 2.7–3.4 emu K mol^{-1} (4.7–5.2 B.M.) given for high spin octahedral monomeric complexes [30]. The decrease in $\chi_m T$ between 300 and ca. 40 K can be ascribed to the spin–orbit coupling present in octahedral Co(II) complexes [23,30], whereas the more abrupt decrease below ca. 40 K may be attributed to the presence of antiferromagnetic exchange interactions between the $[Co(2,2'\text{-bpy})_2]^{2+}$ cations and the V(IV) ions via the bridging oxygen atoms, as can be anticipated from the almost linear V–O–Co bridges.

4. Conclusion

In summary, we have synthesized and characterized two new neutral bicapped bisupporting Keggin-POM derivatives directly constructed from classical Keggin polyoxoanion under hydrothermal conditions. They represent the first example of neural bicapped bisupporting Keggin POMs. Several lines of experimental evidence converge to indicate that the electrochemical behavior of the bicapped bisupporting Keggin POMs is very similar to their parent, undergoing three two-electron redox processes. It may open up the way for comparison between electrochemical behavior of parent POM and transition-metal ion substituted systems.

Supplementary materials

Crystallographic data for the structural analysis have been deposited with the Cambridge Crystallographic Data Centre, CCDC Nos. CCDC 259393 and 260071 for compounds **1** and **2**, respectively. Copies of this information can be obtained free of charge at www.ccdc.cam.ac.uk/conts/retrieving.html [or from the CCDC, 12 Union Road, Cambridge CB2 1EZ, UK; Fax: (internet.) +44 1223/336 033; E-mail: deposit@ccdc.cam.ac.uk].

Acknowledgments

This research was financially supported by the National Science Foundation of China (20271011). We are grateful for the measurements of magnetic susceptibility and helpful discussion provided by Prof. Coronado and Prof. Gomez García of the Institute of Molecular Materials, Department of Inorganic Chemistry, University of Valencia, Spain.

References

[1] V. Soghomonian, Q. Chen, R.C. Haushalter, J. Zubieta, Science 259 (1993) 1596.
[2] Z. Shi, S.H. Feng, S. Gao, L.R. Zhang, G.Y. Yang, J. Hua, Angew. Chem. Int. Ed. 39 (2000) 2325.
[3] O.M. Yaghi., M. O'Keeffe, N.W. Ockwig, H.K. Chae, M. Eddaoudi, J. Kim, Nature 423 (2003) 705.
[4] P.S. Halasyamani, M.J. Drewitt, D. O'Hare, Chem. Commun. (1997) 867.
[5] Y. Wang, J.H. Yu, Y. Du, Z. Shi, Y.C. Zou, R.R. Xu, J. Chem. Soc. Dalton Trans. (2002) 4060.
[6] L. Han, M.C. Hong, R.H. Wang, J.H. Luo, Z.Z. Lin, D.Q. Yuan, Chem. Commun. (2003) 2580.
[7] D. Drewes, E.M. Limanski, B. Krebs, Eur. J. Inorg. Chem. (2004) 4849.
[8] A. Müller, F. Peters, M.T. Pope, D. Gatteschi, Chem. Rev. 98 (1998) 239.
[9] M. Yuan, Y.G. Li, E.B. Wang, C.G. Tian, L. Wang, C.W. Hu, N.H. Hu, H.Q. Jia, Inorg. Chem. 42 (2003) 3670.
[10] S.T. Zheng, J. Zhang, G.Y. Yang, Eur. J. Inorg. Chem. (2004) 2004.
[11] D. Hagrman, C. Zubieta, D.J. Rose, J. Zubieta, R.C. Haushalter, Angew. Chem. Int. Ed. 36 (1997) 873.
[12] L.M. Duan, C.L. Pan, J.Q. Xu, X.B. Cui, F.T. Xie, T.G. Wang, Eur. J. Inorg. Chem. (2003) 2578.
[13] J.Y. Niu, D.J. Guo, J.P. Wang, J.W. Zhao, Cryst. Growth Des. 4 (2004) 241.
[14] X.Y. Wei, M.H. Dickman, M.T. Pope, J. Am. Chem. Soc. 120 (1998) 10254.
[15] W.B. Yang, C.Z. Lu, Inorg. Chem. 41 (2002) 5638.
[16] C.M. Liu, D.Q. Zhang, C.Y. Xu, D.B. Zhu, Solid State Sci. 6 (2004) 689.

[17] C.L. Pan, J.Q. Xu, Y. Sun, D.Q. Chu, L. Ye, Z.L. Lü, T.G. Wang, Inorg. Chem. Commun. 6 (2003) 233.
[18] M. Sadakane, E. Steckhan, Chem. Rev. 98 (1998) 219.
[19] A. Kuhn, F.C. Anson, Langmuir 12 (1996) 5481.
[20] B. Keita, L. Nadjo, J. Electroanal. Chem. 243 (1998) 87.
[21] X.L. Wang, Z.H. Kang, E.B. Wang, C.W. Hu, Mater. Lett. 56 (2002) 393.
[22] X.J. Gu, J. Peng, Z.Y. Shi, Y.H. Chen, Z.G. Han, E.B. Wang, J.F. Ma, N.H. Hu, unpublished work.
[23] O. Kahn, Molecular Magnetism, VCH Publishers, New York, 1993.
[24] C.R. Deltcheff, M. Fournier, R. Franck, R. Thouvenot, Inorg. Chem. 22 (1983) 207.
[25] G.M. Sheldrick, SHELX-97, Program for Crystal Structure Refinement, University of Göttingen, Germany, 1997;
G.M. Sheldrick, SHELXL-97, Program for Crystal Structure Solution, University of Göttingen, Germany, 1997.
[26] Q. Chen, C.L. Hill, Inorg. Chem. 35 (1996) 2403.
[27] I.D. Brown, D. Altermatt, Acta Crystallogr. B 41 (1985) 244.
[28] M.T. Pope, E. Papaconstantinou, Inorg. Chem. 6 (1967) 1147.
[29] E. Cadot, M. Fournier, A. Tézé, G. Hervé, Inorg. Chem. 35 (1996) 282.
[30] R. March, W. Clegg, R.A. Coxall, L. Cucurull-Sánchez, L. Lezama, T. Rojo, P. González-Duarte, Inorg. Chim. Acta 353 (2003) 129.